DOI: 10.1002/cmdc.200700324

pH Effects on the Conformational Preferences of Amyloid β-Peptide (1–40) in HFIP Aqueous Solution by NMR Spectroscopy

Mariacristina Valerio,[a] Fernando Porcelli,[b] Joseph P. Zbilut,[c] Alessandro Giuliani,[d] Cesare Manetti,[a] and Filippo Conti*[a]

The structure and aggregation state of amyloid β-peptide (Aβ) in membrane-like environments are important determinants of pathological events in Alzheimer's disease. In fact, the neurotoxic nature of amyloid-forming peptides and proteins is associated with specific conformational transitions proximal to the membrane. Under certain conditions, the Aβ peptide undergoes a conformational change that brings the peptide in solution to a "competent state" for aggregation. Conversion can be obtained at medium pH (5.0–6.0), and in vivo this appears to take place in the endocytic pathway. The combined use of ^{1}H NMR spectroscopy and molecular dynamics-simulated annealing calculations in aqueous hexafluoroisopropanol simulating the membrane environment, at different pH conditions, enabled us to get some insights into the aggregation process of Aβ, confirming our previous hypotheses of a relationship between conformational flexibility and aggregation propensity. The conformational space of the peptide was explored by means of an innovative use of principal component analysis as applied to residue-by-residue root-mean-square deviations values from a reference structure. This procedure allowed us to identify the aggregation-prone regions of the peptide.

Introduction

Amyloid β-peptide (Aβ) is the main component of amyloid deposits found in the brain of Alzheimer's disease (AD) patients. The peptides, mainly composed of 40 and 42 residue species (Aβ(1–40) and Aβ(1–42), respectively), are normally generated by the proteolytic processing of a larger transmembrane protein, amyloid precursor protein (APP).[1] Although the physiological functions of the Aβ peptide are still under investigation (an antioxidative function has been hypothesized[2]), it is widely believed that the aggregation of Aβ plays a causative role in the pathogenesis of AD.[3,4] Over the past ten years, the central role of Aβ in AD pathogenesis has stimulated many researchers to investigate several properties of Aβ and its variants, including physicochemical properties, secondary structure contents, and fibrillogenic propensity under different conditions. It has been well established that the conformational and aggregation state of Aβ is environment dependent. In general, the Aβ monomer acquires an α-helical structure in membrane or membrane-mimicking environments, and an unstructured conformation in aqueous solutions. In both cases, within the polymeric peptide assembly, the Aβ monomers exist mainly in β-sheet conformation; this points to the need for a striking conformational change from an α-helix or random coil to β-sheet conformation before or following the aggregation process.[5,6] Likewise, other amyloidogenic proteins have been shown to undergo conformational changes leading to the formation of partially folded species with structural features that promote fibril formation. Presumably, these monomeric partially structured intermediates enable the occurrence of specific intermolecular interactions, such as hydrophobic interactions and backbone hydrogen bonding, necessary for oligomerization and fibrillation.[7–11] A detailed picture of the conformational features and mechanism of formation of the partially structured intermediates is still lacking.

The neurotoxic mechanism of partially folded or/and aggregated Aβ and their involvement in AD are the subject of intense debate. Initially, it was hypothesized that the amyloid fibrils were the neurotoxic species (the amyloid cascade hypothesis).[12] Recent evidence have revealed that soluble oligomeric intermediates formed at early stages of aggregation and fibrillization, rather than the mature full-length fibrils, may be the primary cytotoxic species that cause neuronal dysfunction.[13,14] Although the exact mechanism of Aβ neurotoxicity is not yet established, the cytotoxic effects of early intermediates have been correlated with amyloid–cell membrane interactions. This would lead to the formation of nonspecific ion channels, drain-

[a] *M. Valerio, C. Manetti, F. Conti*
Dipartimento di Chimica, Università "La Sapienza", Piazzale Aldo Moro 5, 00185 Roma (Italia)
Fax: (+39) 064455278
E-mail: filippo.conti@uniroma1.it

[b] *F. Porcelli*
Dipartimento di Scienze Ambientali, Università della Tuscia, Largo dell'Università, 01100 Viterbo (Italia)

[c] *J. P. Zbilut*
Department of Molecular Biophysics and Physiology, Rush University Medical Center, 1635 W. Congress, Chicago, IL 60612 (USA)

[d] *A. Giuliani*
Dipartimento Ambiente e Connessa Prevenzione Primaria, Istituto Superiore di Sanità, Viale Regina Elena 299, 00161 Roma (Italia)

Supporting information for this article is available on the WWW under http://www.chemmedchem.org or from the author.

ing cellular energy stores, inhibiting neuronal signaling, and disrupting Ca^{2+} homeostasis.[15–17] This in turn would trigger apoptosis. Based on this finding, Ross and Poirier[14] suggested that the inhibition at early stages of the aggregation pathway would be beneficial to the cell, preventing the formation of potentially toxic intermediates. The knowledge of the structures and the mechanism associated with the conformational transitions preceding protein aggregation at the microscopic level is thus of primary importance.

Previous biophysical studies revealed that Aβ(1–40) forms amyloid fibrils more rapidly at pH 5.0–6.0, near its isoelectric pH, than it does at pH 7.0–7.5 in aqueous buffer;[18] Selkoe et al.[4] reported that Aβ generation from the APP precursor seems to involve an acid cellular organelle. Lysosomal involvement in amyloidogenesis has also been suggested for several other peptides implicated in amyloid disease.[19] Furthermore, several events in vivo, such as a loss of oxygen to cerebral tissues, can cause localized drops in pH favoring aggregation, Yates et al.[20] demonstrated that brains from patients who died after AD are more acidic (pH 6.6) than brains from healthy individuals (pH 7.1). Consequently, an in vitro model system employing the pH range 5.0–6.0 could be not only convenient but also physiologically reasonable to explore Aβ aggregation. NMR conformational studies of the synthetic Aβ peptides in physiological conditions, especially the more aggregation prone Aβ(1–40), have been hampered by problems related to time- and concentration-dependent aggregation. Earlier NMR solution studies have been performed using smaller-sized Aβ peptide, low or high pH, and/or mixture of water and fluorinated alcohols or micellar solutions to overcome the solubility problem and to disrupt quaternary structure and dissociate peptide aggregates.[21–30] Recently some NMR studies on small fragments and on the full length peptides in dilute aqueous solutions, have been reported.[31–34] All these studies suggest that Aβ undergoes substantial conformational changes depending on the environment and can easily convert among disordered, α-helical, and β-strand conformers as a result of a change in solution conditions. Under membrane-mimicking conditions, Aβ contains a significant α-helical character, whereas in physiological buffers a dominant random coil state is observed. Thus, the choice of the solvent is crucial not only to overcome the poor solubility of the Aβ peptide, but also to probe the propensity of monomeric sequences to adopt local structure driving the conformational change for the conversion of soluble peptide into aggregated form. With this aim, hexafluoroisopropanol (HFIP) has been shown to be suitable for detailed structural analysis for these peptides[21,23,24,35] and to create an apolar microenvironment such as the lipid phase of the membrane.[36,37] Several studies have indicated that the aggregation propensity of Aβ variants in aqueous buffer and HFIP/H_2O are similar.[21,35] The HFIP/H_2O mixture is a convenient environment to analyze the pH-dependent conformational changes characterizing the initial events of the aggregation pathway. The presence of fluorinated alcohols favors the stabilization of the monomeric form, and allows monitoring of the more aggregation-promoting condition.[38,39]

We chose to analyze Aβ(1–40) under different pH conditions in the range between 3.5 and 7.0 in the HFIP/H_2O (70/30 *v/v*) mixture. In agreement with our previous studies,[40,41] the results presented herein, indicate a strong correlation between conformational flexibility and propensity to aggregate. The stretches of the sequence with the highest propensity to aggregate were identified as the highly hydrophobic core (Phe19–Ala21) and C-terminal regions (Lys28–Gly38).

Results

Aβ(1–40) structures at different pH

Under our experimental conditions, there was no evidence of aggregation or precipitation for the Aβ(1–40) peptide during the time of NMR measurements. The system AB40L was stable for several months, whereas AB40N and AB40M systems showed changes in the distribution and in the shape of ^1H resonances over several weeks and days, respectively, suggesting the presence of aggregated forms. The aggregation behavior of Aβ(1–40) peptide has been tested by plotting the sum of the signal volumes with chemical shifts between 0 and 1.5 ppm in the ^1H NMR spectra versus time.[56] Figure 1 shows

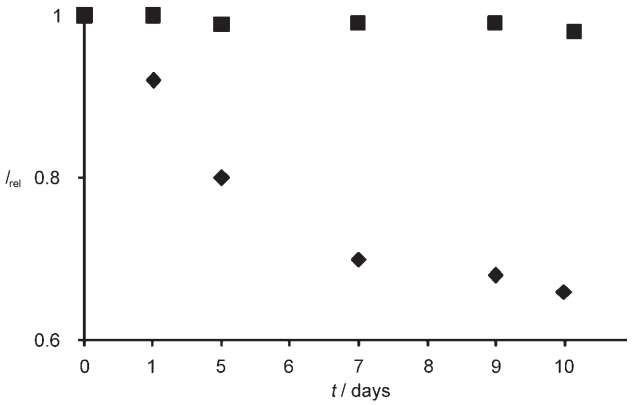

Figure 1. Aggregation behavior of AB40M and AB40N. The sum of the signal volumes with chemical shifts between 0 and 1.5 ppm in the ^1H NMR spectra vs. time elapsed after sample preparation of AB40M (diamond) and AB40N (square) is reported. Signal intensity 1.0 corresponds to the first NMR spectrum recorded.

that the signal intensities were constant for AB40N and decreased for AB40M during the first week.

To assign the backbone and side-chain resonances, a combination of $^1H/^1H$ 2D TOCSY and NOESY spectra at different mixing times were used, according to the standard procedures established by Wüthrich.[49] In Figure 2 two selected NOESY (150 ms mixing time) regions are reported, showing the HN-Hα (top) and the NH–NH (bottom) connectivities for AB40L. From the analysis of the 2D NOESY spectra, as reported in Table 1, we were able to assign 169, 145, and 168 intraresidue and 360, 178, and 341 interresidue NOEs for AB40L, AB40M, and AB40N, respectively. It is worth noting that AB40M revealed a smaller number of NOE contacts. Figure 3 a, b, and c

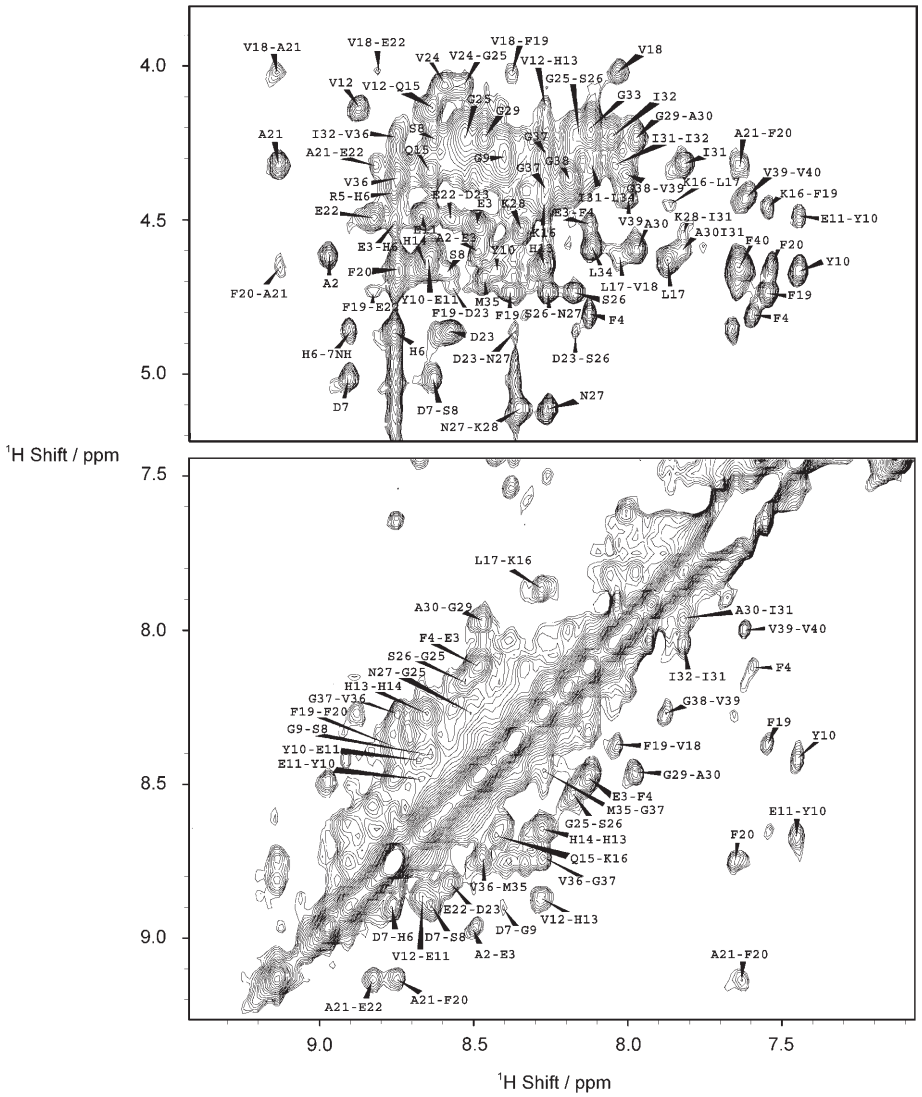

Figure 2. 2D ^{1}H/^{1}H NOESY spectrum of AB40L. Selected regions from a two-dimensional ^{1}H/^{1}H NOESY experiment with a 150 ms mixing time for the Aβ peptide (DAEFRHDSGY EVHHQKLVFF AEDVGSNKGA IIGLMVGGVV) in HFIP/water mixture at pH 3.5: Top HN-Hα and bottom HN-HN regions.

Table 1. NMR constraints and structural statistics of AB40L, AB40M, and AB40N structures.

	AB40L	AB40M	AB40N
Numbers of NOE			
Total	529	323	509
Intra-residue	169	145	168
Inter-residue	360	178	341
Average Energies [kcal mol^{-1}]	20 structures	15 structures	15 structures
E_{tot}	-863 ± 44	-590 ± 50	-790 ± 35
E_{bond}	16 ± 1	17 ± 2	16 ± 2
E_{angle}	64 ± 6	68 ± 15	66 ± 11
$E_{improper}$	14 ± 2	19 ± 3	17 ± 2
E_{VDW}	18 ± 21	35 ± 10	20 ± 8
E_{NOE}	25 ± 9	35 ± 15	35 ± 15
E_{RAMA}	-438 ± 27	-245 ± 30	-375 ± 20
rmsd [Å]			
Backbone Superimposition	0.20 ± 0.10 (Asp7–Val24) 0.12 ± 0.10 (Ile31-Leu34)	0.28 ± 0.18 (Gln15–Val24)	0.27 ± 0.11(Tyr10–Asp23)

show the backbone NOE patterns (top) and the chemical shift indices (CSI) (bottom) for Aβ peptide at different pH environments. Deviations of more than −0.1 ppm of the CSI value, in conjunction with $d_{\alpha N}(i,i+3)$, $d_{\alpha N}(i,i+4)$, and $d_{\alpha\beta}(i,i+3)$ connectivities suggest the presence of an α-helix between residues Tyr10–Asp23 and Ile31–Leu36 in AB40L (Figure 3a). The presence of the Hα-proton of Asn27 shifted downfield suggests that the helix is not continuous from Tyr10 to Leu36, but is broken into two halves. The values of chemical shifts for AB40M and AB40N (Figure 3b and c) are closer to random coil values indicating that the peptide becomes less structured as the pH increases. Analysis of NOE connectivities provides further evidence of a partial unfolding of the two helices. In particular, at pH 5.8, the smaller number of characteristic $d_{\alpha N}(i,i+3)$, $d_{\alpha N}(i,i+4)$, $d_{\alpha\beta}(i,i+3)$, medium-strong $d_{NN}(i,i+1)$, and medium $d_{\alpha N}(i,i+1)$ NOE connectivities mostly in the C-terminal region of the peptide confirms the absence of a well-defined α-helix in this region.

The structures resulting from simulated annealing calculation for AB40L, AB40M, and AB40N are shown superimposed in Figure 4a, b, and c. The heterogeneity within these structures was assessed using the consecutive segment approach, in which the rmsd differences of the backbone atoms for short segments, 2–5 residues in length, were systematically and pairwise compared. Two regions, with well-defined α-helical structure between residues Asp7 and Val24 (rmsd 0.20 ± 0.10) and between Ile31 and Leu34 (rmsd 0.12 ± 0.10) were identified for AB40L (Figure 4a). These structures superimposed on the backbone atoms from residues Asp7 through Leu34 gave a rmsd of 1.78 ± 0.72 Å showing that the

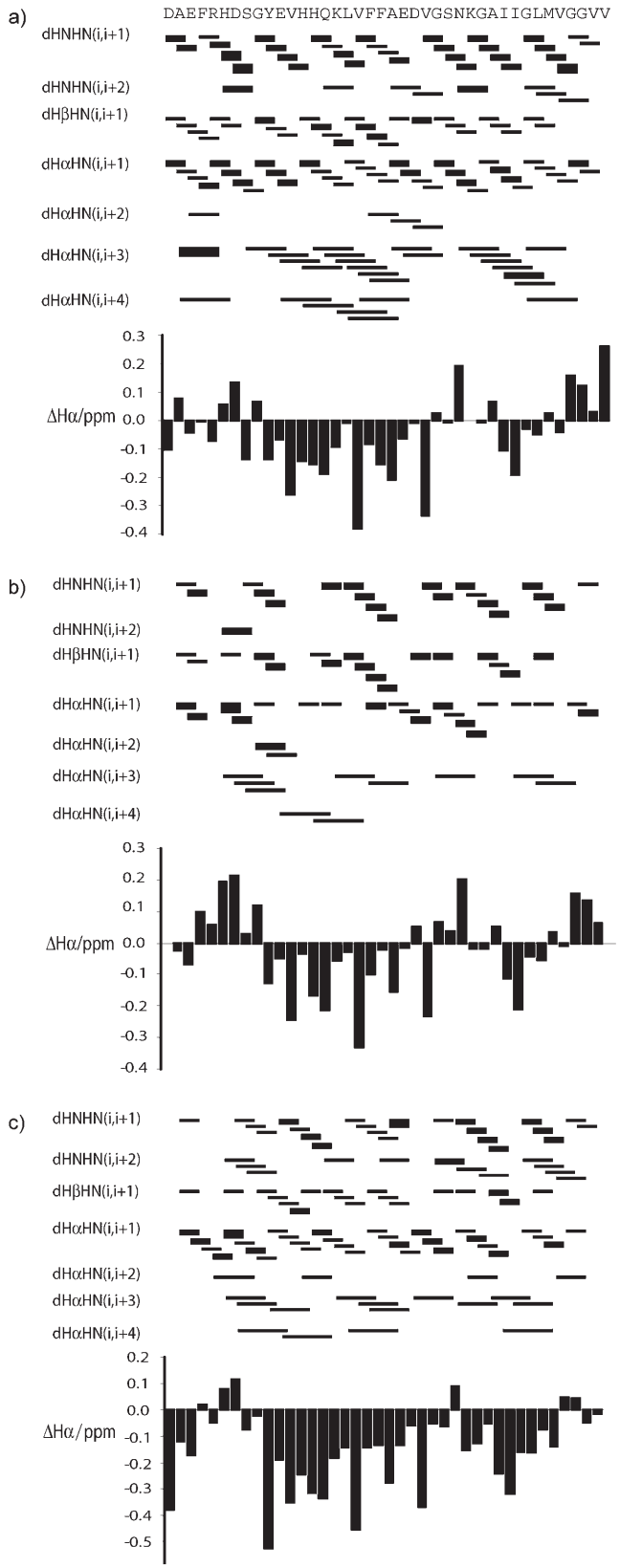

Figure 3. Backbone NOE patterns and the chemical shift indices for Aβ(1–40) peptides. Summary of NMR structural parameters of Aβ-peptides in H_2O/HFIP solution at different pH determined from NMR experiments: a) AB40L, b) AB40M, c) AB40N. In the upper part of the figure the backbone NOE patterns are shown, the correlations indicated with thick lines correspond to strong NOE, whereas correlation indicated with thin lines correspond to medium NOEs. In the bottom part of the figure the CSI are shown.

two domains are connected by a more flexible region. For AB40M and AB40N (Figure 4b and c) only a stable α-helical region extending from residues Gln15 to Val24 and Tyr10 to Asp23, with rmsd values of 0.28 ± 0.18 and 0.27 ± 0.11 Å respectively, was identified. The geometric parameters for the lowest energy structures are summarized in Table 1.

To highlight the structural differences of Aβ(1–40) at different pH conditions, an optimal view may be provided by the secondary structure profile analysis for each set of structures. The percent occurrence of a given secondary structure determined over the final clusters of structures of AB40L, AB40M, and AB40N, as a function of residue number is reported in Figure 4d, e, and f. Table 2 instead reports the percentage of α-helical structure calculated for the entire sequence and the region corresponding to residues Ile31–Gly37. As predicted by qualitative analysis, the secondary structure report, according to DSSP criteria,[53] indicates the presence of two helices for the above regions. At low pH, Aβ(1–40) displays two distinct α-helices from Arg5 to Val24 and from Lys28 to Met35 joined by a very flexible region. The most stable α-helical regions reside between Asp7 to Val24 (helix 1) and Ile31 to Leu34 (helix 2). As the pH increases, the peptide becomes less structured. In the N-terminal region, AB40N adopts an α-helical conformation between residues Tyr10 and Asp23, whereas AB40M is helical only in the segment Gln15–Val24. It can be added that the helix 1 has amphipatic character in AB40M: one face of helix has hydrophobic residues (Leu17, Val18, Phe20, Ala21, and Val24), whereas the other contains polar and charged residues (Gln15, Lys16, Glu22, and Asp23) together with Phe19 (see Figure 5). The C terminus assumes an α-helical folding at pH 3.5, but is disordered at higher pH values. With an increase of pH, helix 2 unfolds more easily than helix 1. However, AB40M reveals a greater conformational flexibility, with helix 2 practically unfolded. The hydrophobic core (Leu17–Ala21) is the most stable region of the peptide at each pH condition.

PCA characterization of the calculated structures

To provide a basis for interpreting structural differences between the AB40M and AB40N ensembles, the two were first analyzed for the scoring of significant differences relative to the phi and psi angles of each of their residues. Statistical comparisons between the experimental groups were performed by unpaired Student's t-test. Differences with a p value of less than 0.05 were considered significant. In Table 3 the t-test for the phi and psi angle means of AB40M and AB40N structures is reported. From the table it is evident that the two ensembles display many significant differences in phi and psi spaces. To come to a systematic understanding of these differences, PCA was employed.

PCA was applied to the data set constituted by the rmsd values calculated for every structure on the Cα atom positions using AB40L average structure as a reference. This produced a 24 unit (conformers) and 40 variable (residues) raw data matrix. PCA of this matrix highlighted a six principal component solution well above the noise floor explaining 77.8% of the total variance. A Student's t-test, applied to PCA scores to

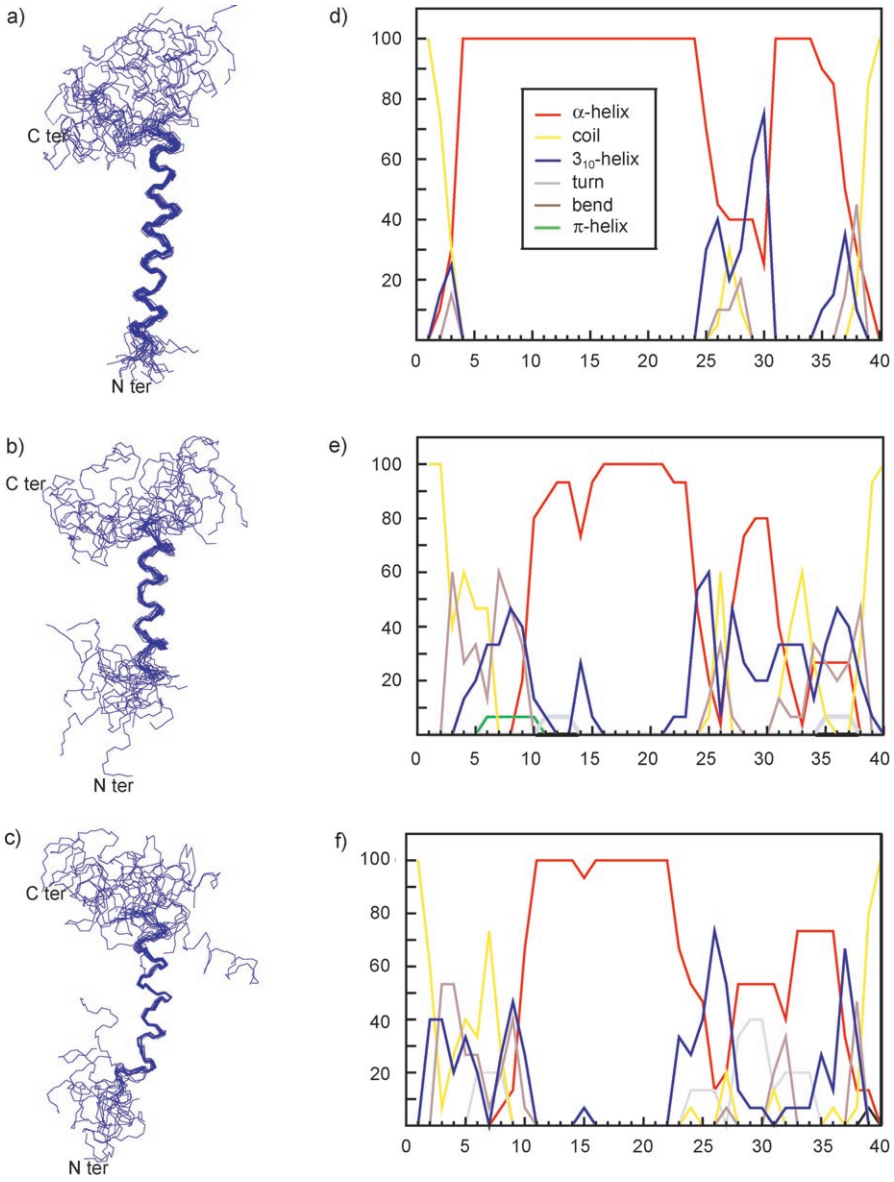

Figure 4. Structural ensembles of Aβ(1–40) peptides. Overlay of the lowest energy structures of Aβ-peptides at different pH calculated from NMR experiments and percentage of secondary structure per residue, according to the DSSP criteria, averaged over the final clusters of structures of AB40L (a and d), AB40M (b and e) and AB40N (c and f).

Table 2. Average percentage of α-helical structure of Aβ(1-40) ensembles at different pH calculated on the entire sequence and between residues Ile31–Gly37.

	Overall	Residues (31–37)
AB40L	78.5 ± 6.0	63.0 ± 11.2
AB40M	47.4 ± 9.7	8.6 ± 13.2
AB40N	53.2 ± 11.4	47.6 ± 29.1

compare the two AB40M and AB40N ensembles of structures, highlights significant differences between the two groups on the first and second principal components (PC1 and PC2, respectively). This can easily be appreciated in Figure 6, where the PCA score plot is reported. A linear discriminant analysis applied to this space allowed for a neat separation of the two groups (Fisher's exact test $p <$ 0.0001). The residues most correlated with PC1 and PC2 (and consequently most influence the separation between AB40M and AB40N structures) are indicated in Table 4 as bolded values. All the loadings (correlation coefficients between components and original variables) on PC1 are positive indicating that all the residues contribute with the same sign to PC1 and can thus be considered as a "weighted cumulative distance" from the reference structure. The weight is assigned in an unsupervised way, with the aim of maximizing the among conformer variability. The recognition that this weighted distance is able to fully discriminate AB40M from AB40N conformers is proof of the fact that the pH conditions are the main order parameter discriminating the different conformers. From the table it is evident that the highly hydrophobic core and C-terminal regions are the crucial patches for discrimination between the two ensembles based on PC1 separation.

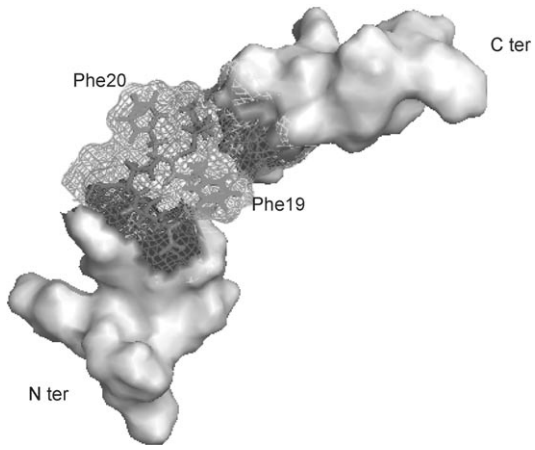

Figure 5. Electrostatic surface potential representation of the AB40M amphipatic helix 1. The helix 1 shows an amphipathic character at pH 5.8. One face of helix 1 has only hydrophobic residues (light gray), whereas the other contains polar and charged residues (dark gray) together with Phe20.

Table 3. T-test for the phi and psi angle means of AB40M and AB40N structures.[a]

	t-test phi	psi
Ala2	0.2644	0.4182
Glu3	0.4965	**0.0330**
Phe4	0.2504	0.7456
Arg5	0.6230	0.7445
His6	**0.0056**	0.9930
Asp7	0.0858	0.3053
Ser8	**0.0381**	**0.0000**
Gly9	0.5564	**0.0490**
Tyr10	0.3058	0.3857
Glu11	0.8442	**0.0000**
Val12	**0.0000**	0.9166
His13	**0.0087**	**0.0045**
His14	**0.0154**	0.9579
Gln15	0.3815	**0.0000**
Lys16	**0.0000**	**0.0000**
Leu17	**0.0000**	**0.0000**
Val18	**0.0000**	**0.0086**
Phe19	0.1506	**0.0000**
Phe20	**0.0004**	**0.0000**
Ala21	0.3252	0.2185
Glu22	0.8285	**0.0455**
Asp23	**0.0007**	0.9461
Val24	0.0970	0.9342
Gly25	**0.0165**	**0.0052**
Ser26	0.1095	**0.0012**
Asn27	0.1095	**0.0012**
Lys28	0.3019	**0.0074**
Gly29	0.1618	0.8361
Ala30	0.8836	0.0652
Ile31	**0.0339**	**0.0207**
Ile32	0.0529	0.8931
Gly33	0.0513	0.3316
Leu34	0.5828	0.8476
Met35	0.3926	0.8861
Val36	0.4767	**0.0283**
Gly37	0.4485	0.4286
Gly38	0.9037	0.5147
Val39	0.6967	0.3753

[a] Any test that results in a *p*-value of less than 0.05 is considered statistically significant and reported in bold.

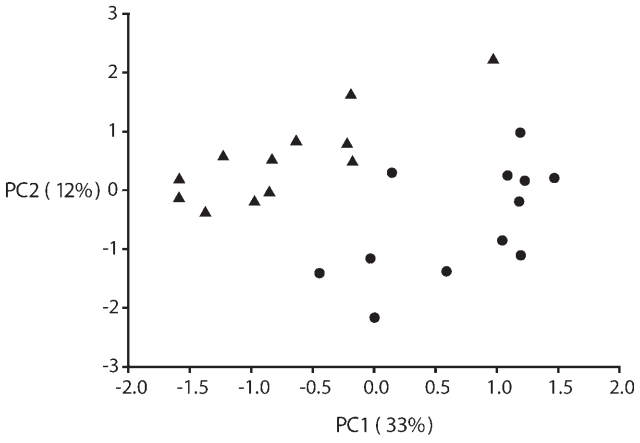

Figure 6. Score plot of factor 1 versus factor 2 of AB40M and AB40N. Plot of the AB40M (circle) and AB40N (triangle) structures in the PCA space spanned by the score of the first and the second latent variables. In parentheses the percent of explained variability is reported.

Table 4. Component loadings relative to the RMSD values of the Cα atom positions of AB40M and AB40N structures calculated respect to AB40L average structure.[a]

Residues	PC 1	PC 2
Asp1	**0.6177**	0.3240
Ala2	**0.6748**	0.3506
Glu3	**0.6579**	0.3628
Phe4	**0.6228**	0.3942
Arg5	0.4956	0.4467
His6	0.4807	0.1376
Asp7	**0.6529**	−0.3241
Ser8	0.4476	−0.3777
Gly9	0.4041	0.1521
Tyr10	0.2577	0.2988
Glu11	**0.7163**	−0.1352
Val12	0.4461	**−0.6065**
His13	0.2404	−0.1859
His14	0.5125	0.3935
Gln15	**0.6992**	−0.2588
Lys16	0.1853	**−0.5273**
Leu17	0.0595	0.4241
Val18	**0.6431**	0.2402
Phe19	**0.7267**	−0.4195
Phe20	0.5238	**−0.6699**
Ala21	**0.6459**	0.3794
Glu22	**0.7305**	−0.1931
Asp23	0.5275	**−0.5901**
Val24	0.3096	−0.0681
Gly25	0.5867	−0.1043
Ser26	0.2408	**0.5581**
Asn27	0.4915	0.1701
Lys28	**0.6953**	0.0780
Gly29	**0.6175**	−0.0894
Ala30	**0.6175**	−0.3485
Ile31	**0.7305**	−0.3535
Ile32	**0.7420**	−0.2891
Gly33	**0.7805**	−0.3289
Leu34	**0.6529**	−0.1175
Met35	**0.7128**	0.2817
Val36	**0.7799**	0.2886
Gly37	**0.6794**	0.2993
Gly38	0.5847	0.2608
Val39	0.4426	0.3544
Val40	0.3648	0.4223

[a] Most relevant loading values for PC1 and PC2, respectively, are reported in bold.

The second component (PC2), at odds with PC1, has both positive and negative loading values, thus it cannot be considered as a cumulative distance but as a geometric shape indicator because bigger distances for some residues (loadings of the same sign) go hand-in-hand with lower distances for others (loadings of opposite sign) pointing to "rigid" shape constraints. From PC2 loading analysis, the presence of geometric constraints between Val12, Lys16, Phe20, and Asp23 in AB40M structures and not in others is indicated by the fact that these residues have loadings of the same sign. To verify whether electrostatic or/and hydrophobic interactions involving these residues could be formed in Aβ(1–40) at pH 5.8 and not in other conditions, we computed the minimum distances between residues within each structure. Table 5 lists the side-chain distances important to discriminate between AB40M and AB40N structures. Interestingly, the distance between Asp23

Table 5. Side-chain contacts among different conformations of Aβ(1–40) peptide.

	Distance (Å)	
	AB40M	AB40N
Residues		
Lys16–Asp23[a]	6.34 ± 3.94	10.88 ± 1.42
Glu22–Lys28[a]	7.82 ± 5.35	4.73 ± 4.22
Asp23–Lys28[a]	11.58 ± 6.35	4.45 ± 3.18
Val12–Lys16[b]	5.92 ± 2.2	2.89 ± 1.1
Phe20–Leu17[c]	4.2 ± 0.5	3.2 ± 0.9
Phe20–Val18[c]	6.2 ± 0.3	6.8 ± 0.2
Phe20–Phe19[c]	4.3 ± 0.5	2.4 ± 0.2
Phe20–Ala21[c]	4.3 ± 0.2	2.9 ± 0.1

[a] The distances were computed between N_ζ of Lys and O_δ of Glu and Asp residues. [b] The distances were computed between NH of Val12 and N_ζ of Lys16 residues. [c] The smallest distances between the side chain of two residues were computed.

and Lys16 in AB40M is on average 58% smaller than the distance in AB40N. Monitoring the pH dependence chemical shift of the β-protons of the residues with carboxyl side chains, we observe the greatest changes for Asp23 as well as Glu22 at pH 5.8–7.0, indicative of higher pK_a values likely due to interaction of the peptide with the cosolvent.[26] Thus, we hypothesized that the deprotonation of the two vicinal residues, Asp23 and Glu22, could weaken the hydrophobically driven fluoroalcohol–peptide association,[38] bringing the side chains of Asp23 and Glu22 into close proximity to those of Lys16 and Lys28 at pH 5.8 and 7.0, respectively. Consequently, at pH 5.8 the distance between the backbone carbonyl oxygen atom of Val12 and the ammonium group of Lys16 increases favoring the unwinding of helix 1 in its N terminus, the side chain of the Phe20 tends to be less packaged in the hydrophobic core and the turn Val24–Lys28, which is centered at amino acid Ser26 and stabilized by the electrostatic interaction involving Lys28 with Glu22 and Asp23 in AB40N, tends to a more extended conformation around Ser26 in AB40M (see Figure 4). Thus, we can interpret PC2 as the image (in terms of relations between distances at different residues) of the electrostatic interaction (constraint) Lys16–Asp23 that is in AB40M but not in AB40N.

The fact that the first PC (that is, the one endowed with the maximal variation explained) is the component that allows for a perfect discrimination of the two conditions, supports the idea that "change of condition" is the main determinant of the variation among conformers, and underscores the overwhelming role of pH in the peptide structure. Moreover the fact that the first PC has positive loadings with all the distances tells us that the effect is relative to the feature of "general flexibility" of the molecule, and that the structural modifications induced by change in pH are relative to the global shape of the molecule and not constrained to specific portions.

Discussion

The important role played by both the structure and aggregation state of Aβ in membrane-like environments in early events leading to Alzheimer's disease is well documented.[57,58,59] It has been widely accepted that, depending on environmental conditions, such as pH, concentration, temperature, ionic strength, metal ions, and so forth, monomeric Aβ can undergo a conformational change to form partially structured intermediates susceptible to fibril formation by a nucleation and growth process.[5,60]

In this work, we determined the structures of Aβ(1–40) in aqueous HFIP solutions at different pH, that has been reported as a model system for aggregation studies.[21,23,24,35]

The secondary structure of Aβ(1–40) is characterized by two helical segments at pH 3.5 between residues Asp7–Val24 and residues Ile31–Leu34 and only one stable α-helix between residues Gln15–Val24 and Tyr10–Asp23 at pH 5.8 and 7.0, respectively. The most relevant structural differences occur in the N-terminal segment and in the highly hydrophobic C-terminal region that are conformationally heterogeneous and are able to adopt helical, disordered, and more extended conformations. It is worth noting that the peptide at pH 5.8, the condition with the highest propensity for aggregation, has the richest conformational flexibility showing the lowest helical content in the hydrophobic tail: 8.6 ± 13.2%, 63.0 ± 11.2%, and 47.6 ± 29.1% for AB40M, AB40L, and AB40N, respectively. Several studies showed that the stabilization of the α-helical content, by mutation of Val18 to Ala in Aβ(1–40), likewise Lys16, Leu17, and Phe20 to Ala in Aβ(1–28), can reduce fibril formation.[61,62] Furthermore, it has been observed that intermediates with partial helical conformation of different Aβ peptides may be on the pathway to fibril formation.[35,63,64,65]

PCA gives further evidence that the peptide in the situation with the highest propensity for fibrillation shows the most flexible structures. The PCA results reveal that AB40M as compared to AB40N is conformationally more distant in terms of rmsd from the reference structures obtained in the most inhibitory condition for aggregation (significantly higher PC1 scores than AB40N). The patches of the central hydrophobic core and highly hydrophobic C-terminal region of the Aβ(1–40) sequence are particularly important to differentiate between AB40M and AB40N. The major conformational flexibility at pH 5.8 appears to regulate the presence of hydrophobic patches at the surface of the molecule, thus giving to Aβ(1–40) the potential to aggregate. Tcherkasskaya et al.[66] found that hydrophobic interactions at early stages promote oligomeric conformations without the characteristic β-sheet structure found in the mature amyloid fibrils. It has been shown that residues in the segment Lys16–Phe20 are essential for Aβ fibril formation, which is prevented by the substitution of these residues.[67–74] These findings are supported by other studies on short amyloidogenic peptides revealing the presence of aromatic residues in their primary sequence and suggesting a primary role for π-stacking interactions in the amyloid formation process.[75–79] Likewise, it has been suggested that the highly hydrophobic C-terminal region is mainly responsible for Aβ aggregation and seeding.[80–84]

The major conformational flexibility in Aβ(1–40) at pH 5.8 could be related to the formation of an electrostatic interaction between Lys16 and Asp23 that may act as a hub letting the extremes free to move and unpackaging the aromatic side

chain of Phe20 from the hydrophobic core. It is worth noting that the Lys16–Asp23 electrostatic contact causes the destabilization of the turn structure in the central region (Val24–Lys28) stabilized by the Glu22–Lys28 and Asp23–Lys28 electrostatic interaction at pH 7.0. This loop structure is implicated in nucleating monomer folding. Lazo et al.[85] hypothesized that the partial unfolding of this region may be necessary for the subsequent oligomerization of Aβ. Fraser et al.[86] found that Lys16 and especially Asp23 are necessary for β-sheet formation. Interestingly, the authors indicated that charge–charge interactions function in concert with hydrophobic interactions to stabilize the β-sheet conformation and assembly of amyloid fibers.

Our results are consistent with earlier data that emphasize the importance of Glu22 and Asp23 in controlling Aβ folding or fibril formation with respect to environmental conditions. Increase in the rate of fibril growth is observed in Aβ peptides with amino acids substitutions linked to familial AD mutations, including Glu22–Gly (Artic),[87] Glu22–Gln (Dutch),[88] Glu22–Lys (Italian),[89] and Asp23–Asn (Iowa).[90] Several authors report that replacements of Asp23 by neutral residues as well as its racemization in the Aβ(1–40) peptide significantly retard fibrillogenesis.[64,91] On the contrary, isomerization of Asp23 in Aβ-(1–42) increases fibril formation.[92] Coles et al.,[26] from NMR studies in solution, observed that at pH 5.8–7.0, in a water/SDS micelle environment, the Aβ(1–40) undergoes a structural transition from α-helix to random coil probably related to the deprotonation of residues Glu22 and Asp23. More significantly, Petkova et al.,[92] based on solid state NMR, proposed a structural model for Aβ(1–40) fibrils showing the mutual interaction between hydrophobicity and charge effect. The electrostatic interaction involving Asp23 and Lys28 favors the sidechain–sidechain interactions between the two β-strands (residues Val12–Val24 and Ala30–Val40) stabilizing the structure of the cross-β unit. Further, if protofibrils associate laterally, an intermolecular electrostatic interaction between Lys16 and Glu22 would also prevent electrostatic destabilization.

Hence, we propose that the difference in conformational flexibility, determined by an interplay between hydrophobicity distribution and side-chain ionization effects, produces a difference in the aggregation propensity. This hypothesis is also strengthened by other investigations regarding some amyloidogenic peptides showing metastable and flexible intermediates along the aggregation pathway.[79,94–96]

Another intriguing implication of the calculated structures is the unfolding of helix 1 into its N terminus, thus conferring an amphipatic character to the peptide at pH 5.8. As a consequence, the calculated structures characterized by an helix-kink-helix motif and the amphipatic character of helix 1 share a common shape to that of the fusion domain of influenza virus Hemagglutinin (HA), the structurally and functionally best studied example of class I membrane fusion proteins.[97,98] Furthermore, the structures obtained for AB40M are similar to those of the theoretical model proposed by Durell et al.[99] for ion channels that might be formed by Aβ(1–40).[100] Based on these structural homologies, it seems fair to suggest that, as recently proposed by other authors,[24,26] the membrane poration process may be relevant to explain the neurotoxicity of Aβ. The amphipatic nature of helix 1 could favor interactions with the membrane surface, thus ensuring an insertion of the hydrophobic residues into lipid bilayer. The ability of Aβ(1–40) to insert into a lipid bilayer by its C terminus[100,101] and the observation of a conformational change into partially α-helical structures of Aβ(1–40) upon membrane incorporation support this hypothesis.[64,103]

Nevertheless, a general model for the membrane interaction of soluble proteins postulates that adoption of a mobile, highly dynamic, conformation confers to the protein the ability to associate.[104] The possibility of a flexible intermediate functioning in the protein insertion was proposed by Bychova and described for a number of systems.[105–108]

In summary, our results show that Aβ(1–40) peptide in an aqueous mixture of HFIP at different pH exhibits a conformational transition from α-helical to more extended conformations with increasing pH. The most involved segment in this conformational change is the highly hydrophobic C-terminal region, which in part loses its helical character. PCA, applied to our knowledge for the first time to multidimensional data of analogous conformations as derived from NMR data, allows, as suggested in a previous paper,[39,40] for the recognition of conformational flexibility, influenced by both hydrophobicity and charge effect, as the main determinant of aggregation propensity. This application of PCA confirms the usefulness of the proposal by Carugo[109] of the systematic use of rmsd as a quantitative metric for structural comparison of different molecules. In his paper he makes use of the Pearson correlation coefficient between rmsd values of different molecules, whereas we start from there and use the eigenvectors of the correlation matrix corresponding to the principal components. This allows us to decompose the global displacement from the reference molecule of each conformer into a "global unconstrained linear displacement" (measured by the first component in which all the residues of the peptide contribute with the same sign to the general distance) and a "local constrained nonlinear displacement" (second component, some residues get closer to the reference while at the same time others get further away because of the presence of shape constraints in the molecule) components. This decomposition allows for a closer look to the nature of the observed phenomenon.[110] Moreover the downsizing of the initial dimensionality of distance space from 40 (the number of residues) to two (the number of components) permits the direct projection of the single conformers into an explicit conformational space, allowing for a much simpler quantitative comparison of the two populations of structures.

In the condition with the highest propensity for aggregation, the formation of a turn-like structure at region Lys16–Asp23 promotes a rich conformational flexibility in the peptide. This flexibility exposes large patches of hydrophobic surface at the central core and at the hydrophobic tail and an amphipatic helical character thus modifying the ability of Aβ(1–40) to either aggregate and/or become inserted in membranes. Furthermore, the common helix-kink-helix shaped amphipatic character of Aβ(1–40) at pH 5.8 with membrane-inserting proteins together with its reported membrane-inserting protein

and ion-channel properties point to membrane poration as one of the possible events for neurotoxicity.

Finally, the detailed characterization of the possible conformational transition leading from the nonaggregating helical structures to partially folded intermediates, could be useful to design molecules able to block the aggregation process at early stages.

Experimental Section

Sample Preparation

Aβ(1-40) (MW 4329.8), purity 82.4%, was purchased from Neosystem (Lyon, France) and purified using reverse-phase high-performance liquid chromatography (RP-HPLC). Purified peptide was stored as lyophilized at −20 °C. The solvent deuterated hexafluoroisopropanol (d_2-HFIP) (98%) was obtained from Aldrich Chemical Co.

1D-NMR experiments were used to optimize the experimental conditions. Aβ(1–40) was dissolved in HFIP/H_2O mixtures at different concentrations 30/70, 40/60, 50/50, 60/40, 70/30, and 80/20 by volume, and optimal line shapes and intensities were obtained using 70% HFIP.

Three different samples were prepared for a final concentration of 300 μM in 0.7 mL of a mixture by volume of d_2-HFIP/H_2O/D_2O (70:27:3) at pH values of 3.5, 5.8, and 7.0 referred to as AB40L, AB40M, and AB40N, respectively. The desired pH values were obtained by adding amounts of either DCl (0.1 M) or NaOD (0.1 M) and measured at room temperature with a pH meter (Radiometer Copenhagen PHM 28). No corrections of pH readings were made for isotopic effects or for the presence HFIP-d, as control experiments showed that these substances did not significantly alter the pH.[33,42]

NMR Spectroscopy

All solution ^{1}H NMR experiments were performed at 25 °C on a Bruker Avance 500 spectrometer. The 2D TOCSY[43] and NOESY[44] spectra were run in the phase-sensitive mode using time-proportional phase increment for quadrature detection in the direct dimension.[45] The 2D [^{1}H, ^{1}H] total correlation spectroscopy (TOCSY) (70 and 80 ms mixing time) and 2D [^{1}H, ^{1}H] NOESY (80-220 ms mixing time) experiments were collected using 2048 complex data points in the direct dimension and 512 increments in the indirect dimension. The solvent signal was suppressed by WATERGATE.[46] Spectral data were processed using NMRPipe[47] and analyzed using SPARKY.[48] Data were zero-filled to 4096 points in F2 and to 1024 points in F1 and then processed with a sine-bell squared window function shifted by between 90° and 60° as appropriate before Fourier transformation. Polynomial baseline correction was carried out on either side of the residual water signal. Spectra were assigned using standard assignment techniques.[49] The identified spin systems were then assigned along the primary structure of the peptides through inter-residue sequence from the NOESY spectrum. In the NOESY (150 ms mixing time) spectra, NOE crosspeaks were integrated and used for structure calculations. The NOE volumes were calibrated using the average NOE volume from resolved aromatic vicinal protons of Tyr10 and classified as strong, medium, and weak, corresponding to distance restraints of 1.9–2.7, 1.9–3.3, and 1.9–5.0 Å, respectively.[50] The spectra were internally referenced to the HDO peak according to the method of Wishart.[51]

Structure Calculation and Validation

Structure calculations were performed starting from extended structures and using the random simulated annealing routine available in XPLOR-NIH[52] to generate 70 conformers. An initial high-temperature phase consisting of 6000 restrained molecular dynamics steps of 0.5 fs each was performed at a temperature of 1000 K. During this stage, all force constants were kept fixed. A molecular dynamics cooling phase composed of 3000 steps of 0.5 fs each was then employed, with the temperature decreasing from 1000 to 100 K. To refine the generated conformers, simulated annealing was carried out a second time starting at 2000 K, including the full van der Waals potential. The temperature was decreased from 2000 to 0 K. During the high temperature steps, the dihedral angles were constrained using an harmonic potential with a force constant of 200 kcal mol^{-1}. Final refinement of the structure ensemble was calculated at a T_i of 500 K with 30000 cooling steps at a step size of 1 fs. All NOEs were unambiguously assigned and pseudoatoms were employed where appropriate using the center of mass approach when stereospecific assignments could not be made. Conformers with no NOE violations >0.4 Å, no bond violations >0.05 Å, and no angle violations $>4°$ were accepted using the "accept.inp" routine included in the XPLOR-NIH software package.

Structural analyses were performed using XPLOR-NIH macros, the defined secondary structure of proteins (DSSP)[53] criteria and in-house developed programs. The MOLMOL program[54] was employed to examined visually the calculated structures.

Statistical Analysis

Principal component analysis (PCA) was applied to visualize significant conformational changes such as those expected for the effects of pH on the structural transition of Aβ peptide. The PCA projects multidimensional data onto low-dimensional space by selecting a new set of mutually orthogonal axes (principal components) that best preserve the distance between the conformations in the original space.[55] In this way, it is possible to directly visualize the spatial relations among the data points representing the different conformers. We used the root-mean-square deviations (rmsd) of the Cα atoms as the distance measure between conformations relative to different experimental conditions. These distances were the original variables entering PCA. The pattern of loadings (normalized eigenvectors) on the extracted components allows for an identification of the nature of the structural modifications. On the other hand, the scores on the components allow for an immediate visualization of the different conformers. SAS (Statistical Advanced Software) software (SAS Institute Inc., Cary, NC) was used for the statistical analysis.

Keywords: Alzheimer's disease · amyloid β-peptides · conformational flexibility · NMR spectroscopy · principal component analysis

[1] H. G. Lemaire, J. M. Salbaum, G. Multhaup, J. Kang, R. M. Bayney, A. Unterbeck, K. Beyreuther, B. Müller-Hill, *Nature* **1987**, *325*, 733–736.
[2] M. A. Smith, C. A. Rottkamp, A. Nunomura, A. K. Raina, G. Perry, *Biochim. Biophys. Acta Mol. Basis Dis.* **2000**, *1502*, 139–144.
[3] D. H. Small, C. A. McLean, *J. Neurochem.* **1999**, *73*, 443–449.
[4] D. J. Selkoe, *Annu. Rev. Neurosci.* **1994**, *17*, 489–517.
[5] L. C. Serpell, *Biochim. Biophys. Acta Mol. Basis Dis.* **2000**, *1502*, 16–20.
[6] O. S. Makin, L. C. Serpell, *FEBS J.* **2005**, *272*, 5950–5961.
[7] R. Gerber, A. Tahiri-Alaoui, P. J. Hore, W. James, *J. Biol. Chem.* **2006**, *282*, 6300–6307.

[8] C. N. Chirita, E. E. Congdon, H. Yin, J. Kuret, *Biochemistry* **2005**, *44*, 5862–5872.
[9] I. Pallares, J. Vendrell, F. X. Aviles, S. J. Ventura, *J. Mol. Biol.* **2004**, *342*, 321–331.
[10] V. N. Uversky, *J. Biomol. Struct. Dyn.* **2003**, *21*, 211–234.
[11] R. Khurana, J. R. Gillespie, A. Talapatra, L. J. Minert, C. Ionescu-Zanetti, I. Millett, A. L. Fink, *Biochemistry* **2001**, *40*, 3525–3535.
[12] J. Hardy, D. Allsop, *Trends Pharmacol. Sci.* **1991**, *12*, 383–388.
[13] C. Haass, D. J. Selkoe, *Nat. Rev. Mol. Cell Biol.* **2007**, *8*, 101–112.
[14] C. A. Ross, M. A. Poirier, *Nat. Med.* **2004**, *10*, S10–S17.
[15] J. I. Kourie, A. L. Culverson, P. V. Farrelly, C. L. Henry, K. N. Laohachai, *Cell Biochem. Biophys.* **2002**, *36*, 191–208.
[16] M. Stefani, C. M. Dobson, *J. Mol. Med.* **2003**, *81*, 678–699.
[17] F. M. LaFerla, *Nat. Rev. Neurosci.* **2002**, *3*, 862–872.
[18] D. G. Lynn, S. C. Meredith, *J. Struct. Biol.* **2000**, *130*, 153–173.
[19] P. Westermark, *Amyloid* **1994**, *1*, 47–60.
[20] C. M. Yates, J. Butterworth , M. C. Tennant, A. Gordon, *J. Neurochem.* **1990**, *55*, 1624–1630.
[21] S. Tomaselli, V. Esposito, P. Vangone, N. A. Van Nuland, A. M. Bonvin, R. Guerrini, T. Tancredi, P. A. Temussi, D. Picone, *ChemBioChem* **2006**, *7*, 257–267.
[22] G. Shanmugam, R. Jayakumar, *Biopolymers* **2004**, *76*, 421–434.
[23] A. M. D'Ursi, M. R. Armenante, R. Guerrini, S. Salvadori, G. Sorrentino, D. Picone, *J. Med. Chem.* **2004**, *47*, 4231–4238.
[24] O. Crescenzi, S. Tommaselli, R. Guerrini, S. Salvadori, A. M. D'Ursi, P. A. Temussi, D. Picone, *Eur. J. Biochem.* **2002**, *269*, 5642–5648.
[25] H. Shao, S. C. Jao, K. Ma, M. G. Zagorsky, *J. Mol. Biol.* **1999**, *285*, 755–773.
[26] M. Coles, W. Bicknell, A. A. Watson, D. P. Fairlie, D. J. Craik, *Biochemistry* **1998**, *37*, 11064–11077.
[27] K. J. Marcinowski, H. Shao, E. L. Clancy, M. G. Zagorsky, *J. Am. Chem. Soc.* **1998**, *120*, 11082–11091.
[28] A. A. Watson, D. P. Fairlie, D. J. Craik, *Biochemistry* **1998**, *37*, 12700–12706.
[29] J. Talafous, K. J. Marcinowsky, G. Kloman, M. G. Zagorsky, *Biochemistry* **1994**, *33*, 7788–7796.
[30] S. A. Poulsen, A. A. Watson, D. P. Fairlie, D. J. Craik, *J. Struct. Biol.* **2000**, *130*,142–152.
[31] L. Hou, H. Shao, Y. Zhang, H. Li, N. K. Menon, E. B. Neuhaus, J. M. Brewer, I. L. Byeon, D. G. Ray, M. P. Vitek, T. Iwashita, R. A. Makula, A. B. Prybyla, M. G. Zagorski, *J. Am. Chem. Soc.* **2004**, *126*, 1992–2005.
[32] J. P. Lee, E. R. Stimson , J. R. Ghilardi, P. W. Mantyh, Y. Lu , A. M. Felix, W. Llanos, A. Behbin, M. Cummings, M. Van Criekinge, W. Timms, J. E. Maggio, *Biochemistry* **1995**, *34*, 5191–5200.
[33] M. G. Zagorski, C. J. Barrow, *Biochemistry* **1992**, *31*, 5621–5631.
[34] J. Jarvet, P. Damberg, K. Bodell, L. E. G. Eriksson, A. Graslund, *J. Am. Chem. Soc.* **2000**, *122*, 4261–4268.
[35] P. Juszczyk , S. Kolodziejczyk, Z. Grzonka, *Acta Biochim. Pol.* **2005**, *52*, 425–431.
[36] T. Sugihara, E. R. Blout, B. A. Wallance, *Biochemistry* **1982**, *21*, 3444–3452.
[37] H. Sticht, P. Bayer, D. Willbold, S. Dames, C. Hilbich, K. Beyreyther, R. W. Frank, P. Rosch, *Eur. J. Biochem.* **1995**, *233*, 293— 298.
[38] R. Rajan, S. K. Awasthi, S. Bhattachajya, P. Balaram, *Biopolymers* **1997**, *42*, 125—128.
[39] S. Bhattacharjya, J. Venkatraman, A. Kumar, P. Balaram, *J. Pept. Res.* **1999**, *54*, 100–111.
[40] J. P. Zbilut, A. Colosimo, F. Conti, M. Colafranceschi, C. Manetti, M. Valerio, C. L. Webber, Jr., A. Giuliani, *Biophys. J.* **2003**, *85*, 3544–3557.
[41] M. Valerio. A. Colosimo, F. Conti, A. Giuliani, A. Grottesi, C. Manetti, J. P. Zbilut, *Proteins Struct. Funct. Genet.* **2005**, *58*, 110–118.
[42] C. J. Barrow, A. Yasuda, P. T. Kenny, M. G. Zagorski, *J. Mol. Biol.* **1992**, *225*, 1075–1093.
[43] A. Bax, D. G. Davis, *J. Magn. Reson.* **1985**, *65*, 335–360.
[44] J. Jeener, B. H. Mayer, P. Bachman, R. R. Ernst, *J. Chem. Phys.* **1979**, *71*, 4546–4553.
[45] D. Marion, K. Wuthrich, *Biochem. Biophys. Res. Commun.* **1983**, *113*, 967–971.
[46] M. Piotto, V. Saudek, V. Sklenar, *J. Biomol. NMR* **1992**, *2*, 661–665.
[47] F. Delaglio, S. Grzesiek , G. Vuister, G. Zhu, J. Pfeifer, A. Bax, *J. Biomol. NMR* **1995**, *6*, 227–293.
[48] T. D. Goddard, D. G. Kneller, SPARKY 3, University of California, San Francisco, **1999**.
[49] K. Wuthrich, *NMR of Proteins and Nucleic Acids*, Wiley, New York, **1986**.
[50] G. C. K. Roberts, *NMR of macromolecules* (Eds.: D. Rickwood, B. D. Hames), IRL, New York, **1993**.
[51] D. S. Wishart, B. D. Sykes, F. M. Richards, *Biochemistry* **1992**, *31*, 1647–1651.
[52] C. D. Schwieters, J. J. Kuszewski, N. Tjandra, G. M. Clore, *J. Magn. Reson.* **2003**, *160*, 65–73.
[53] W. Kabsch, C. Sanders, *Biopolymers* **1983**, *22*, 2577–2637.
[54] R. Koradi, M. Billeter, K. Wüthrich, *J. Mol. Graphics* **1996**, *14*, 51–55.
[55] R. Benigni, A. Giuliani, *Am. J. Physiol.* **1994**, *266*, R1697–R1704.
[56] R. Riek, P. Günter, H. Döbeli, B. Wipf, K. Wüthrich, *Eur. J. Biochem.* **2001**, *268*, 5930–5936.
[57] N. Arispe, E. Rojas, H. B. Pollard, *Proc. Natl. Acad. Sci. USA* **1993**, *90*, 567–571.
[58] D. H. Cribbs, C. J. Pike, S. L. Weinstein, P. Velazquez, C. W. Cotman, *J. Biol. Chem.* **1997**, *272*, 7431–7436.
[59] M. J. Widenbrant, J. Rajadas, C. Sutardja, G. G. Fuller, *Biophys. J.* **2006**, *91*, 4071–4080.
[60] D. Thirumalai, D. K. Klimov, R. I. Dima, *Curr. Opin. Struct. Biol.* **2003**, *13*, 146–159.
[61] C. Soto, E. M. Castano, B. Frangine, N. C. Inestrosa, *J. Biol. Chem.* **1995**, *271*, 3063–3067.
[62] L. O. Tjenberg, J. Näslund, F. Lindqvist, J. Johansson, A. R. Karlström, J. Thyberg, L. Terenius, C. Nordstedt, *J. Biol. Chem.* **1996**, *271*, 8545–8548.
[63] A. Päiviö, E. Nordling, Y. Kallberg, J. Thyberg, J. Johansson, *Protein Sci.* **2004**, *13*, 1251–1259.
[64] M. D. Kirkitadze, M. M. Condron, D. B. Teplow, *J. Mol. Biol.* **2001**, *312*, 1103–1119.
[65] Y. Fezoui, D. B. Teplow, *J. Biol. Chem.* **2002**, *277*, 36948–36954.
[66] O. Tcherkasskaya, W. Sanders, V. Chynwat, E. A. Davidson, C. S. Orser, *J. Biomol. Struct. Dyn.* **2003**, *21*, 353–365.
[67] C. Hilbich, B. Kisters-Woike, J. Reed, C. L. Masters, K. Beyreuther, *J. Mol. Biol.* **1991**, *218*, 149–163.
[68] C. Hilbich, B. Kisters-Woike, J. Reed, C. L. Masters, K. Beyreuther, *J. Mol. Biol.* **1992**, *228*, 460–473.
[69] S. J. Wood, R. Wetzel, D. J. Martin, M. R. Hurle, *Biochemistry* **1995**, *34*, 724–730.
[70] W. P. Esler, E. R. Stimson, J. R. Ghilardi, Y. Lu, A. M. Felix, H. V. Vinters, P. W. Mantyh, J. P. Lee, J. E. Maggio, *Biochemistry* **1996**, *35*, 13914–13921.
[71] D. S. Fay, A. Fluet, C. J. Johnson, C. D. Link, *J. Neurochem.* **1998**, *71*, 1616–1625.
[72] S. A. Poulsen, A. A. Watson, D. P. Fairle, D. J. Craig, *J. Struct. Biol.* **2000**, *130*, 142–152.
[73] C. Wurth, K. Guimard, M. Hecht, *J. Mol. Biol.* **2002**, *319*, 1279–1290.
[74] E. Gazit, *Curr. Med. Chem.* **2002**, *9*, 1725–1735.
[75] Y. B. Zhang, W. Swietnicki, M. G. Zagorsky, W. K. Surewicz, F. D. Sonnichsen, *J. Biol. Chem.* **2000**, *275*, 33650–33654.
[76] M. Reches, Y. Porat, E. Gazit, *J. Biol. Chem.* **2002**, *277*, 35475–35480.
[77] R. Azriel, E. Gazit, *J. Biol. Chem.* **2001**, *276*, 34156–34161.
[78] Y. Mazor, S. Coilead, I. Benhar, E. Gazit, *J. Mol. Biol.* **2002**, *322*, 1013–1024.
[79] A. Mascioni, F. Porcelli, U. Ilangovan, A. Ramamoorthy, G. Veglia, *Biopolymers* **2003**, *69*, 29–41.
[80] J. T. Jarrett, E. P. Berger, P. T. Lansbury, *Biochemistry* **1993**, *32*, 4693–4697.
[81] P. T. Lansbury, P. R. Costa, J. M. Griffiths, E. J. Simon, M. Auger, K. J. Halverson, D. A. Kocisko, Z. S. Hendsch, T. T. Ashburn, R. G. S. Spencer, B. Tidor, R. G. Griffin, *Nat. Struct. Biol.* **1995**, *2*, 990–998.
[82] C. J. Pike, A. J. Walencewicz-Wasserman, J. Kosmoski, D. H. Cribbs, C. G. Glabe, C. W. Cotman, *J. Neurochem.* **1995**, *64*, 253–265.
[83] H. Döbeli, N. Draeger, G. Huber, P. Jakob, D. Schmidt, B. Seilheimer, D. Stuber, B. Wipf, M. Zulauf, *Nat. Biotechnol.* **1995**, *13*, 988–993.
[84] D. B. Teplow, *Amyloid* **1998**, *5*, 121–142.
[85] N. D. Lazo, M. A. Grant, M. M. Condron, A. C. Rigby, D. B. Teplow, *Protein Sci.* **2005**, *14*, 1581–1596.
[86] P. E. Fraser, D. R. McLachlan, W. K. Surewicz, C. A. Mizzen, A. D. Snow, J. T. Nguyen, D. A. Kirschner, *J. Mol. Biol.* **1994**, *244*, 64–73.

[87] C. Nilsberth, A. Westlind-Danielsson, C. Eckman, M. M. Condron, K. Axelman, C. Forsell, C. Stenh, J. Luthman, D. B. Teplow, S. G. Younkin, J. Naslund, L. Lannfelt, *Nat. Neurosci.* **2001**, *4*, 887–893.
[88] E. Levy, M. D. Carman, I. J. Fernandez-Madrid, M. D. Power, I. Lieberburg, S. G. van Duinen, G. T. Bots, W. Luyendijk, B. Frangione, *Science* **1990**, *248*, 1124–1126.
[89] L. Miravalle, T. Tokuda, R. Chiarle, G. Giaccone, O. Bugiani, F. Tagliavini, B. Frangione, J. Ghiso, *J. Mol. Biol.* **2000**, *275*, 27110–27116.
[90] T. J. Grabowski, H. S. Cho, J. P. G. Vonsattel, G. W. Rebeck, S. M. Greenberg, *Ann. Neurol.* **2001**, *49*, 697–705.
[91] T. Tomiyama, S. Asano, Y. Furiya, T. Shirasawa, N. Endo, H. Mori, *J. Biol. Chem.* **1994**, *269*, 10205–10208.
[92] T. Shimizu, N. Izumiyama, S. Murayama, H. Fukuda, T. Shirasawa, *Soc. Neurosci. Symp.* **2000**, *26*, 1284.
[93] A. T. Petkova, Y. Ishii, J. J. Balbach, O. N. Antzutkin, R. D. Leapman, F. Delaglio, R. Tycko, *Proc. Natl. Acad. Sci. USA* **2002**, *99*, 16742–16747.
[94] F. Bemporad, G. Calloni, S. Campioni, G. Plakoutsi, N. Taddei, *Acc. Chem. Res.* **2006**, *39*, 620–627.
[95] S. Zhang, K. Iwata, M. J. Lachenmann, J. W. Peng, S. Li, E. R. Stimson, Y. Lu, A. M. Felix, J. E. Maggio, J. P. Lee, *J. Struct. Biol.* **2000**, *130*, 130–141.
[96] A. Ahmad, I. S. Millett, S. Doniach, V. N. Uversky, A. L. Fink, *Biochemistry* **2003**, *42*, 11404–11416.
[97] X. Han, J. H. Bushweller, D. S. Cafiso, L. K. Tamm, *Nat. Struct. Biol.* **2001**, *8*, 715–720.
[98] Y. Li, X. Han, L. A. Lai, J. H. Bushweller, D. S. Cafiso, L. K. Tamm, *J. Virol.* **2005**, *79*, 12065–12076.
[99] S. R. Durell, H. R. Guy, N. Arispe, E. Rojas, H. B. Pollard, *Biophys. J.* **1994**, *67*, 2137–2145.
[100] Y. J. Zhu, H. Lin, R. Lal, *FASEB J.* **2000**, *14*, 1244–1254.
[101] R. Brasseur, *Mol. Membr. Biol.* **2000**, *17*, 31–40.
[102] S. R. Ji, Y. Wu, S. Sui, *J. Biol. Chem.* **2002**, *277*, 6273–6279.
[103] D. M. Walsh, D. M. Hartley, Y. Kusumoto, Y. Fezoui, M. M. Condron, A. Lomakin, G. B. Benedek, D. J. Selkoe, D. B. Teplow, *J. Biol.Chem.* **1999**, *274*, 25945–25952.
[104] M. W. Parker, F. Pattus, *Trends Biochem. Sci.* **1993**, *18*, 391–395.
[105] V. E. Bychkova, R. H. Pain, O. B. Ptitsyn, *FEBS Lett.* **1988**, *238*, 231–234.
[106] E. London, *Biochim. Biophys. Acta Rev. Biomembr.* **1992**, *1113*, 25–51.
[107] A. Muga, J. M. González-Manás, J. H. Lakely, F. Pattus, W. K. Surewicz, *J. Biol. Chem.* **1993**, *268*, 1553–1557.
[108] S. Bañuelos, A. Muga, *Biochemistry* **1996**, *35*, 3892–3898.
[109] O. Carugo, *Protein Eng. Des. Sel.* **2007**, *20*, 33–37.
[110] J. N. Darroch, J. E. Mosimann, *Biometrika* **1985**, *72*, 241–252.

Received: November 12, 2007
Revised: December 19, 2007
Published online on January 28, 2008

